45th AIAA Aerospace Sciences Meeting and Exhibit
8 - 11 January 2007, Reno, Nevada

AIAA 2007-801

Numerical Simulation of Effects of Buoyancy on Wake Instability of Heated Cylinder in Contra Flow

Khyati B. Varma[1] and Hui Hu[2] and Z J Wang[3]
Iowa State University ,Ames, Iowa, 50011

Flow over a cylinder is a classical and practically interesting problem. A number of studies focus on the vortex shedding and wake instability of an unheated cylinder. Inspite of its applications flow over a heated cylinder operating in a mixed convection region has received very little attention. The present study aims at the numerical investigation of unsteady heat transfer for a laminar flow past a circular cylinder with small aspect ratio (L/D=7) or finite spanwise length with no-slip wall conditions . A circular cylinder is exposed to approaching flow stream in the direction of gravity or opposing the direction of buoyant force (contra flow). The Reynolds number and the temperature of the incoming flow are set as Re=130 and 297 K respectively. The temperature of the heated cylinder is varied between 297 K to 358 K corresponding to Richardson number varying between Ri=0.0 and Ri=1.05. The analysis performed focuses on the effect of buoyancy on the wake instability in terms of vortex shedding frequency, drag forces, wake centerline velocities, averaged Nusselt number and transition phenomenon. In addition to this, a preliminary study is conducted to understand the influence of small aspect ratio and end effects on the transition mechanism due to heating. Numerical results are compared to available experimental data and some new results are presented.

Nomenclature

D	=	diameter of the cylinder
L	=	length of the cylinder
x,y,z	=	cartesian co-ordinates
V_∞	=	Uniform inlet streamwise velocity
u	=	crossflow velocity component
v	=	streamwise velocity component
w	=	spanwise velocity component
V_c	=	mean velocity in streamwise direction
$\overline{D}$	=	time-averaged drag
$\overline{p}$	=	mean pressure
$\overline{C_d}$	=	time-averaged drag co-efficient
f	=	frequency of vortex shedding
Gr	=	Grashof number
Ri	=	Richardson number
Re	=	Reynolds number
St	=	Strouhal number
T_w	=	cylinder wall temperature
T_∞	=	temperature of water

[1] Graduate Student, Department of Aerospace Engineering, and AIAA Student Member, email: khyati@iastate.edu.
[2] Assistant Professor, Department of Aerospace Engineering, and AIAA Senior Member.
[3] Associate Professor, Department of Aerospace Engineering. and AIAA Associate Fellow.

g = gravitational acceleration
β = thermal expansion coefficient of water
C_p = specific heat of water
k = thermal conductivity of water
ρ = density of water
μ = dynamic viscosity of water
$\overline{Nu}$ = averaged Nusselt number
$\overline{Q}$ = heat flux

I. Introduction

FOR over a century, the wake flow behind a cylinder has captivated the attention of scientists and engineers (Williamson [1], Hatton [3], Oosthuizen et al. [4], Badr [7]). Flow over a cylinder results in the vortex shedding phenomenon over a wide range of Reynolds Number ($\mathrm{Re} = \rho V_\infty D / \mu_\infty$). A number of studies focus on the wake stability and vortex shedding characteristics for an unheated cylinder for low Reynolds Number. In the last decade, researchers have worked in the field of 3D wake dynamics behind an unheated cylinder with advances in experimental and numerical studies.

After a review of the literature on wake flow behind unheated and heated cylinder, the present study aims at the numerical investigation of flow over a heated cylinder in a contra (vertically downward) flow arrangement and the effect of buoyancy on the wake behind it. The heat induced buoyancy effects are expressed by Grashof number ($Gr = g\beta(T_w - T_\infty)D^3 / \nu_\infty^2$) and the relative importance of the forced and buoyant effects is indicated by Richardson number ($Ri = Gr / \mathrm{Re}^2$). With the increasing Ri the heat transfer process around the heated cylinder changes from forced convection to the mixed convection regime.

Williamson [1] concluded from his experiments that for an unheated cylinder, the flow becomes 3D when the Re is greater than 180. However the 3D behavior can be observed for even a lower Re if the aspect ratio of the cylinder L/D is low with the cylinder of a finite length. The results presented by Williamson [1] vary for the aspect ratio less than 28 and larger aspect ratios. Similar behavior is observed by Mittal [2] and the end conditions determine the mode of vortex shedding for a finite cylinder. His studies indicate that the wake transition regime that is known to exist in the Re range of 190-250 for large aspect-ratio cylinders is either extended and/or delayed for a cylinder of small aspect-ratio with "no-slip" walls. In the current study, the aspect-ratio AR of L/D=7, is used to faithfully model the experimental conditions. For such an aspect ratio and Re, the wake transition regime is extended which is presented here. The results for 3D transition are discussed for Re=130 and *Ri =0.0 to 1.05* and the results are analyzed to study how the heating would affect the transition mechanism. Vortex shedding becomes very complicated, when the buoyant forces take over the viscous phenomenon. This classical and practically interesting phenomenon has its implications in other applications such as heat exchanger tubes, nuclear reactor fuel rods, chimney stack, cooling towers, offshore structures, electronics cooling etc. A number of engineering design parameters connected with fluid flow and heat transfer become important in these studies. Apart from engineering relevance, a study of these mechanisms associated with the laminar flow past cylinders, forms the first step towards the understanding of vastly more complicated phenomenon of turbulence.

Researchers investigated the buoyancy effects for the first time in early seventies to study the influence of the induced heat on the heat transfer coefficient (Hatton [3]). This study gave remarkable results for critical Ri being more than 0.2 due to the influence of thermal effects for various angles between the gravity vector and the streamwise direction. Oosthuizen et al. [4] have studied the influence of mixed convection over a Reynolds number range of 100-300 with their interest in calculating the average heat transfer. Jain et al. [5] have pointed out an increase in the vortex shedding frequency with increasing cylinder temperature. Furthermore, investigations for thermal effects on the wake by Noto et al. [6] and Badr [7] described the flow over a horizontal heated cylinder opposing the direction of gravity. The results by Noto et al. [6] indicated the effect of increasing cylinder temperature on the Strouhal Number. According to them, the Strouhal number decreases to almost zero after a critical Richardson number. The same situation was numerically analysed by Chang and Sa [8] with detailed study on the vortex mechanisms in the near wake of a heated/cooled circular cylinder in a parallel flow (vertically upwards). With the recent development in this area, Kieft and Steehoven [9] have studied the effect of buoyancy on

the heated cylinder in a horizontal cross flow. From their studies they found that the non-parallelism between the crossflow and buoyant forces cause the flow pattern to become asymmetric.

Most recently, Hu and Koochesfahani [10] have done an experimental investigation of the effect of buoyancy on the wake instability of a heated cylinder in a contra flow. So far, there is no published literature on the numerical investigation of the same problem. In the present study, special attention is given to the analysis of buoyancy effects on the wake instability of the heated cylinder in terms of vortex shedding frequency, the wake closure length, drag coefficient and the local and averaged Nusselt number of the heated cylinder. We know that non-intrusive flow visualization experimental techniques like Laser-Induced Fluorescence (LIF), Particle Image Velocimetry (PIV) etc. turn out to be very expensive. On the other hand CFD simulation of such a problem can give us a preliminary understanding of the flow physics at a much lower cost.

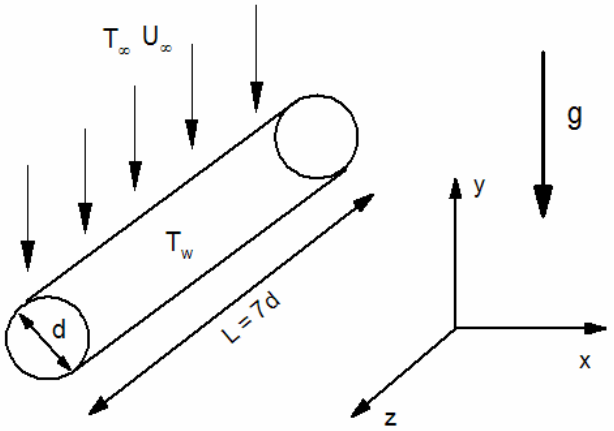

Figure 1. Schematic of approaching flow over cylinder

The main objective of the present study is the numerical simulation of unsteady-state heat transfer for a laminar flow past a circular cylinder. The analysis performed focuses both, on the 3D flow transition and the wake instability due to buoyancy effects. A circular cylinder is exposed to approaching flow stream in the direction of gravity or opposing the direction of buoyant flow. The Reynolds number and the temperature of the incoming flow are set as $\mathrm{Re}=130$ and $24^{\circ}C$ respectively. The temperature of the heated cylinder is varied between $24^{\circ}C$ to $85^{\circ}C$ corresponding to Richardson number varying between $Ri=0$ and $Ri=1.0$. When the temperatures of the cylinder and flow stream are the same, an isothermal wake develops behind the cylinder. However, when the cylinder temperature is higher than the flow stream temperature, a wake with buoyant force opposing the flow stream direction occurs. In addition to this, special attention is given to the influence of small aspect ratio (AR) and end effects on the transition mechanism due to heating.

II. Methodology

A. Problem Definition

For a fixed value of Reynolds number $\mathrm{Re}=130$, at varying Richardson number $\mathrm{Ri}=0.0\,\mathrm{to}\,1.0$, both unsteady two-dimensional and three-dimensional flow simulations for water have been carried out trying to maintain similar characteristics of mesh generation and solver set-up to make the results comparable. The flow is assumed to be in the vertically downward direction approaching the isothermal heated copper cylinder as shown in the schematic of the problem in Fig. 1. The six cases for various temperature conditions of the heated cylinder that are studied in the present work are listed in the Table 1.

Table 1. The six studied cases with the controlling parameters

Case No.	T_w and T_∞	Reynolds number $\mathrm{Re}=\frac{\rho V_\infty D}{\mu_\infty}$	Grashof number $Gr=\frac{g\beta(T_w-T_\infty)D^3}{\nu_\infty^2}$	Richardson number $Ri=\frac{Gr}{\mathrm{Re}^2}$
1	$T_w = 24^oC$, $T_\infty = 24^oC$	130	0	0.00
2	$T_w = 35^oC$, $T_\infty = 24^oC$	130	3300	0.19
3	$T_w = 42^oC$, $T_\infty = 24^oC$	130	5400	0.31
4	$T_w = 53^oC$, $T_\infty = 24^oC$	130	8700	0.50
5	$T_w = 66^oC$, $T_\infty = 24^oC$	130	12500	0.72
6	$T_w = 85^oC$, $T_\infty = 24^oC$	130	18200	1.05

B. Computational Modeling and Numerical Method

In the current study, numerical investigation has been conducted using a time-accurate finite-volume method solving the unsteady Navier-Stokes equations. The commercial finite volume computational fluid dynamics code, FLUENT 6.0 is used for the numerical simulation. Spatial derivatives were discretized using QUICK scheme which is based on averaging the second order upwind and central differences of a variable. The second-order implicit method was used for temporal discretization. The segregated solver was applied to solve the momentum and the energy equations and considering the difference of thermophysical properties between the fluid region and the cylinder, the double-precision solver is used. At each step, the momentum equations are first solved to obtain the velocity field. The pressure field and velocity field were coupled by PISO (Pressure Implicit with Splitting Operator) method. Upon solving the continuity and momentum equations, the energy equation was solved to achieve a quasi-steady periodic condition. The lift force was monitored over the cylinder surface as a function of time. The steady-periodic state was assumed to be achieved when the variation in the oscillating amplitudes of the C_d was less than 1%. The time step size can be calculated based on the vortex shedding frequency for the unheated cylinder in terms of the Strouhal Number. Based on the previous experimental and numerical results, we know that the Strouhal Number for flow past an unheated cylinder for Re=150 is approximately 0.18. In order to capture the shedding correctly, we need atleast 20 to 25 time steps in one shedding cycle. A thorough time refinement study is performed based on the above calculations and used consistently for all the simulations.

1. Mesh Generation

As discussed earlier, the aspect-ratio of the cylinder used for the present study is low which results in end effects due to no-slip boundary condition. This leads to a 3D transition in the wake for the present Re=130 even for the unheated case. Hence we cannot use a two-dimensional grid for our numerical simulation. The two-dimensional simulations were performed mainly to verify the consistency of the choices related to the computational domain dimensions and to its discretization. The computational domain is meshed using CFD-GEOM into a quadratic mesh. To obtain a structured mesh, domain decomposition in sub-volumes is needed and has been implemented as shown in the Fig. 2.

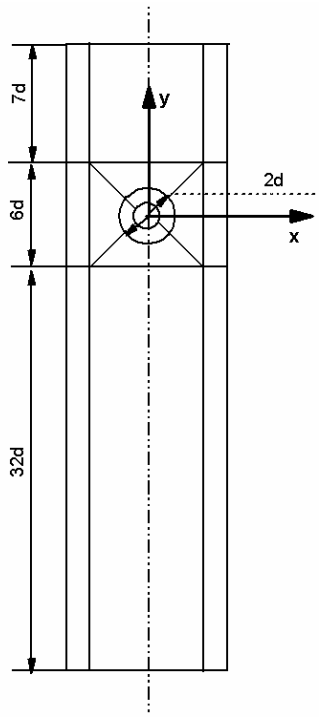

Figure 2. Domain Decomposition

Accuracy of CFD solutions strongly depends on the grid system which must be constructed to minimize the grid-induced errors and to resolve the flow physics. For this purpose a final grid system (Fig. 3) is employed after generating solutions on three different grid systems illustrated in the Table 3. The result of the assessment of this grid independence study is represented in Table 3, for the predicted values of the vortex shedding frequency of Strouhal Number. The correct reproduction of the St for the unheated cylinder is achieved indicating grid independence until the variations in the St were less than 2.0% which compares fairly well with the experimental results. Table 3, demonstrates that the fine grid yields the most grid independent result based on the criteria for St. Every solution present in this work is made grid independent in the manner described above.

As mentioned earlier, two-dimensional numerical results remain far from the physical phenomenon when the cylinder has a finite length or the aspect-ratio is low. This conclusion is clearly evident in Fig. 8 and Fig. 13. in the since 3D modes arise in the cylinder wake for even for Ri=0.00 and are extended for higher Ri. The assessment of this result is demonstrated in detail in the results for Strouhal number and mean velocity profiles for 2D simulations for both unheated and heated cases. The mesh generation for the 3D model is a clear extension of the 2D one. The length of the cylinder is about 7D to model the experimental settings in Hu et al. [10]. The possibility of extruding the superficial mesh in the spanwise direction allows the use of wall boundary condition for the lateral walls. Also assuming that the flow is symmetric about the center plane (transverse plane), in the spanwise direction (z-direction), a symmetry boundary condition can be used for the center plane. This reduces the total number of cells

Table 3.Grid convergence using Strouhal Number

Mesh Density	*No. of cells*	*St*
Coarse	13249	0.17781
Medium	22224	0.17423
Fine	32391	0.17116

and in turn the computational time by half.

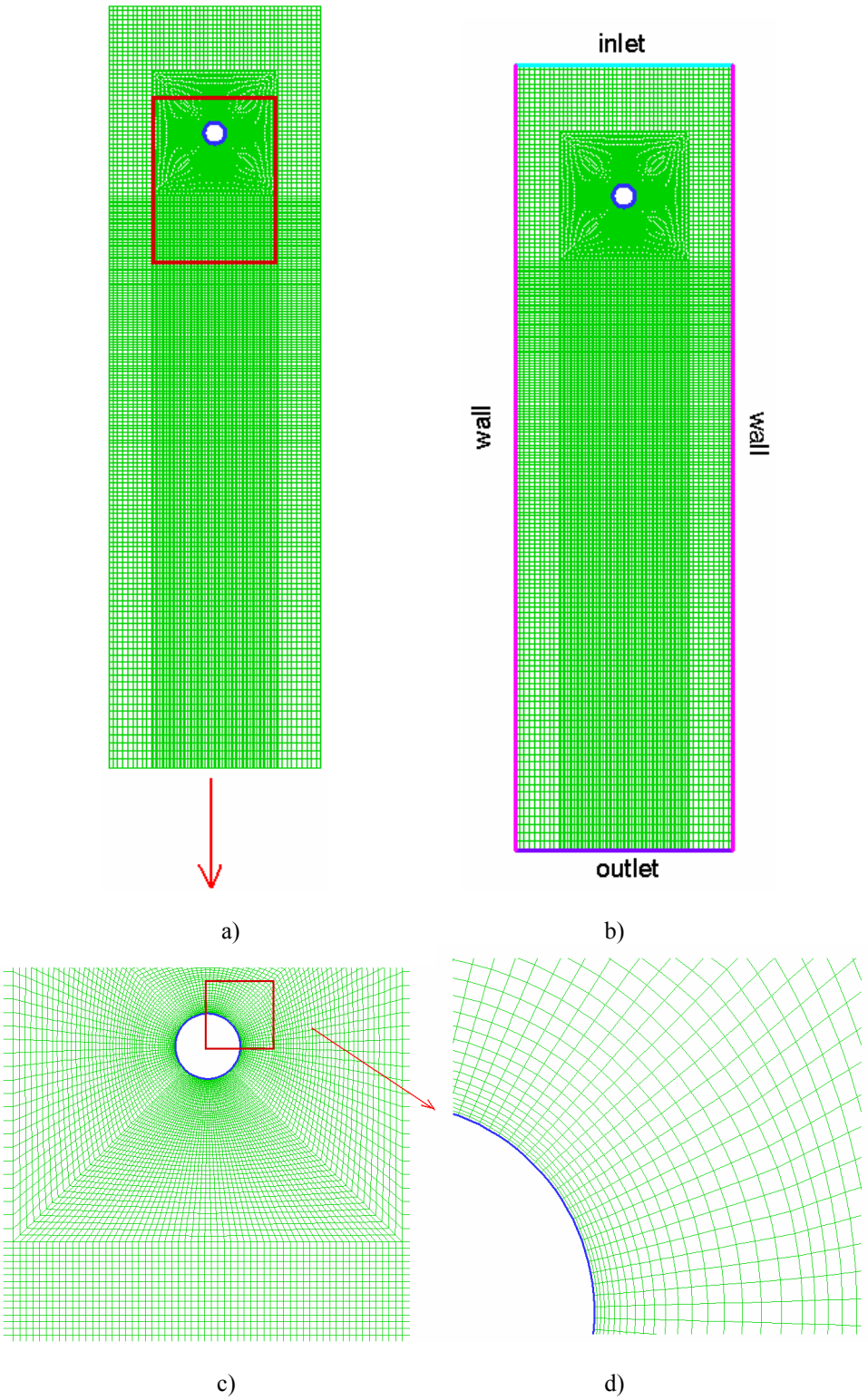

Figure 3. 2D grid system

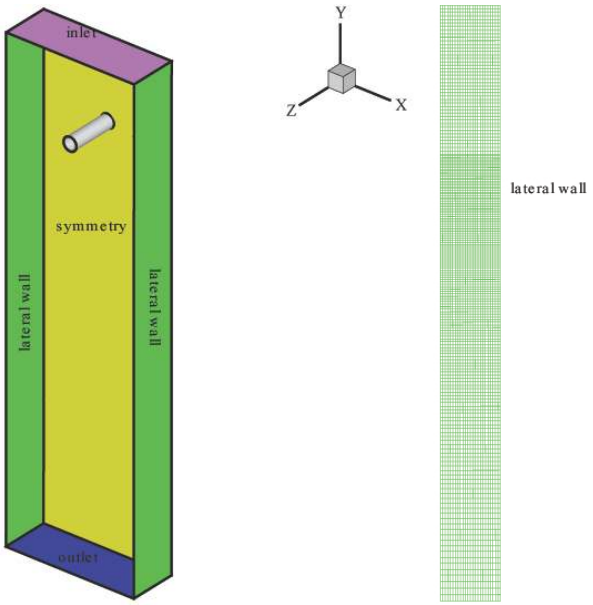

Figure 4. 3D grid system

2. Boundary Conditions

The boundary conditions for the computational domain can be specified as follows. At the inlet, uniform velocity and temperature boundary conditions were imposed. The inlet freestream velocity $V_\infty = 0.0255 m/\sec$ as calculated for $\mathrm{Re} = 130$ considering the thermophysical properties of water at over cylinder temperature T_∞=297 K or $24°C$ based on the definition of Re.

$$\text{u=0, v=}V_\infty,\ T_\infty\text{=297 K} \tag{1}$$

A pressure outlet condition is specified at the outlet. With this type of boundary condition, the input pressure is used as the static pressure of the fluid at the outlet plane and all other conditions are extrapolated from the interior of the domain.

For the lateral boundaries, the no-slip condition is applied with adiabatic thermal wall boundary condition.

$$\text{u=v=w=0 and T=}T_\infty \tag{2}$$

The no-slip boundary condition was applied at the isothermal test cylinder where constant wall temperature condition is modeled. Based on $\mathrm{Ri} = 0.0 \text{ to } 1.0$, the temperature T_w of the copper cylinder ranges from $297K - 358K$ ($24°C - 85°C$).

$$\text{u=v=w=0 and T=}T_w \tag{3}$$

3. Properties of water and copper

The thermophysical properties of water vary with the temperature. The thermally induced variation of the material properties of water cannot always be safely neglected over this range $292K - 360K$. For instance, the viscosity assumes almost 67% variation from $989 \times 10^{-6}\ Ns/m^2$ to 324×10^{-6} in the temperature range of $292K - 360K$. Hence polynomial functional relations are used to account for the temperature dependence. The following equations are used to determine variation with the temperature in density, specific heat, thermal conductivity and dynamic viscosity of water.(Incropera and DeWitt [13]). These formulae are implemented in the numerical computation with the user defined functions (UDFs).

$$\rho = \frac{a_0 + a_1 T + a_2 T^2 + a_3 T^3 + a_4 T^4 + a_5 T^5}{1 + a_6 T} \tag{4}$$

$$C_p = b_0 + b_1 T + b_2 T^2 + b_3 T^3 + b_4 T^4 \tag{5}$$

$$k = c_0 + c_1 T + c_2 T^2 + c_3 T^3 + c_4 T^4 \tag{6}$$

$$\mu = d_0 + d_1 T + d_2 T^2 + d_3 T^3 + d_4 T^4 \tag{7}$$

The coefficients of temperature dependence for density, specific heat, thermal conductivity and viscosity are in Table 2. corresponding to Eqs [4-7] respectively.

Table 2. Coefficients in temperature dependence formulae

n	a_n	b_n	c_n	d_n
0	1819	1.6987	1.8231	46763
1	-12.105	-0.024932	-0.020442	-510.93
2	7.04×10^{-2}	1.469×10^{-4}	1.0365×10^{-4}	2.2991
3	-1.9675×10^{-4}	-4.3376×10^{-7}	-2.0506×10^{-7}	-4.602×10^{-3}
4	2.601×10^{-7}	6.4132×10^{-10}	1.396×10^{-10}	3.4604×10^{-6}
5	-1.3494×10^{-10}			

4. 2D numerical simulations

2D simulations help us to analyze the influence of the domain size and grid resolution. It has also highlighted that to obtain the correct vortex shedding frequency; a fine circumferential discretization is needed even for the unheated case. All the meshes both for 2D and 3D models are structured with quadrilateral and hexahedral cells respectively. The choice is tied to the need of using higher order numerical schemes available in FLUENT, only for such type of grids.

Table 4. 2D simulation settings

Settings	*Choice*
Simulation	2D
Solver	Segregated implicit, Unsteady, Laminar
Temporal Discretisation	Second order
Pressure	QUICK
Momentum equation	QUICK
Pressure-Velocity coupling	PISO
Energy equation	QUICK
Inlet boundary condition	Velocity Inlet
Outlet boundary condition	Pressure outlet
Lateral wall boundary condition	Wall
Total cells amount	32391

It will be discussed later in the results section that the wake behavior is no more 2D in nature if the AR is low. This makes the results obtained from the 2D simulations difficult to interpret and validate.

5. 3D numerical simulations

The 3D numerical settings are as represented in the Table 5. As described earlier, the 3D model is an extension of the 2D model with all the solver settings and spatial and temporal discretization consistent with the 2D simulation settings. In the sections to follow all the results for both 2D and 3D simulations are discussed.

Table 5. 3D simulation settings

Settings	*Choice*
Simulation	3D
Solver	Segregated Implicit, Unsteady, Laminar
Temporal Discretization	Second order
Pressure	QUICK
Momentum equation	QUICK
Pressure-Velocity coupling	PISO
Energy	QUICK
Inlet boundary condition	Velocity Inlet
Outlet boundary condition	Pressure outlet
Lateral wall boundary condition	Wall
Centerplane boundary condition	Symmetry
Total cells amount	689164

III. Results and Discussions

A. Streamlines and Contours

Streamlines indicate the flow pattern at a given instant of time. The influence of buoyancy on the fluid flow in the wake region is shown by plotting the instantaneous streamlines shown in Fig. 5, for Ri=0.00 and Ri=1.05. Here the separation angle θ_{sep}, measured from the forward stagnation point is higher for Ri=0.0. The wake region is marked by a zone of reverse flow very near the cylinder surface, which can be seen in form of negative streamwise velocity vectors due to the existence of the recirculation zone downstream of the cylinder (Fig. 6). With the increasing temperature of the cylinder (*Ri*), the separation angle θ_{sep}, decreases since the direction of the flow and buoyancy oppose each other. This results in a wider wake and the recirculation zone for heated cylinder case becomes longer than the unheated cylinder. The near wake patterns, thus obtained can be seen in Fig. 7. As can be observed, the vortex shedding pattern for the unheated cylinder (Ri=0.0) is severely altered by the buoyant force.

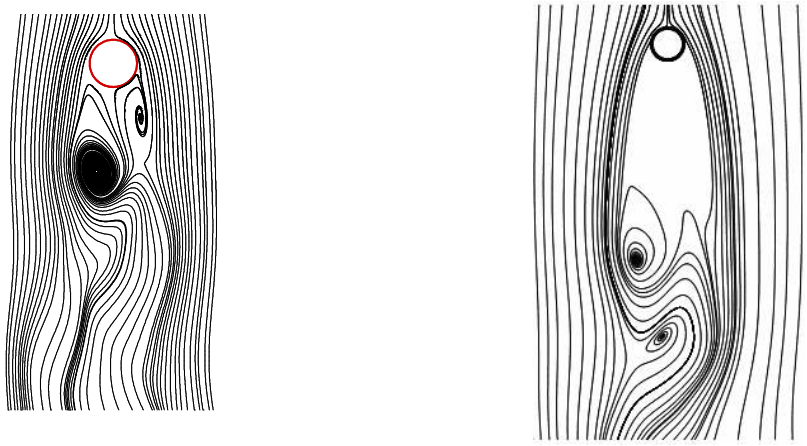

(a) Ri=0.0 **(b) Ri=1.05**

Figure 5. Computational Instantaneous streamlines

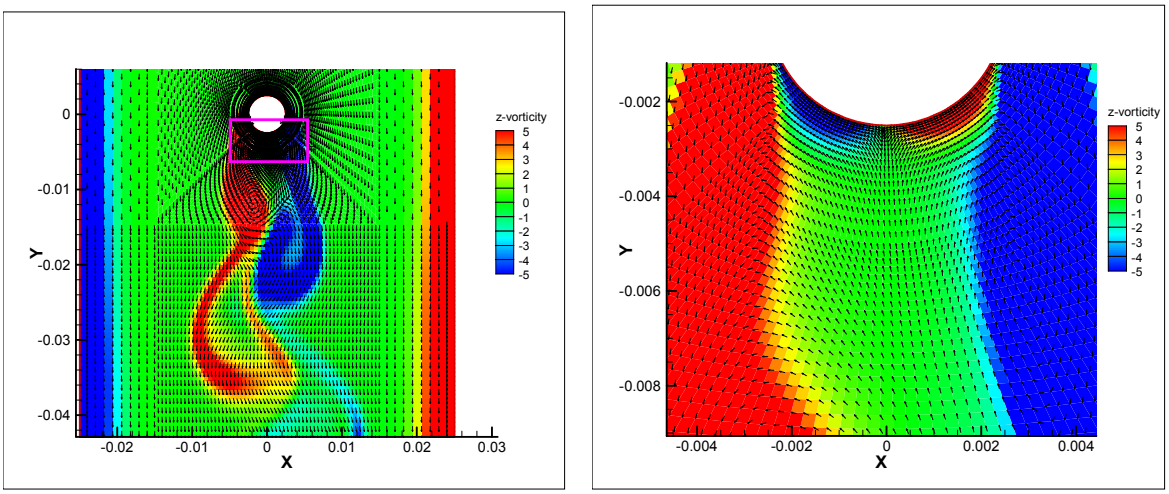

Figure 6. z-Vorticity near the cylinder Ri=0.0

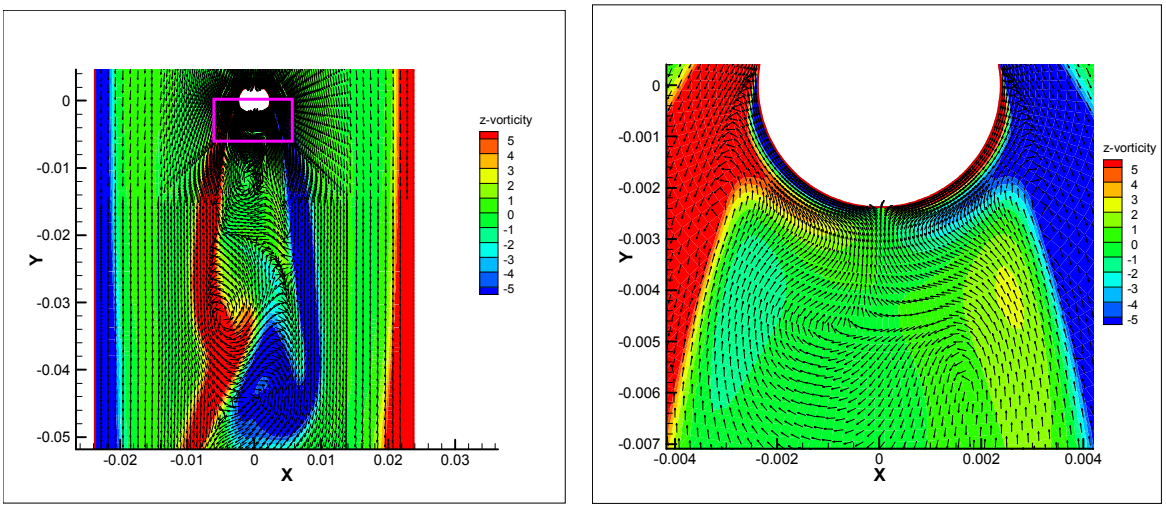

Figure 7. z-vorticity near the cylinder Ri=1.05

B. Time-averaged wake centerline velocities

Numerical results for the time-averaged mean center line velocities along the vertical axis of the cylinder in the wake region on the symmetry plane are shown in Fig. 9, for *Ri=0.00, Ri=0.72* and *Ri=1.05*. The experimental observations of Hu et al. [10] are also presented for the purpose of comparison. As discussed earlier, the wake region is marked by a zone of reverse flow very near the cylinder surface be seen in the form of negative velocity values due to the existence of the recirculation zone downstream of the cylinder. But the wake behavior strongly depends on the end conditions. If we have a no-slip wall boundary condition as our end conditions for cylinders with low AR, we are certain to see 3D wake behavior even for Re<180 as mentioned earlier Mittal [2]

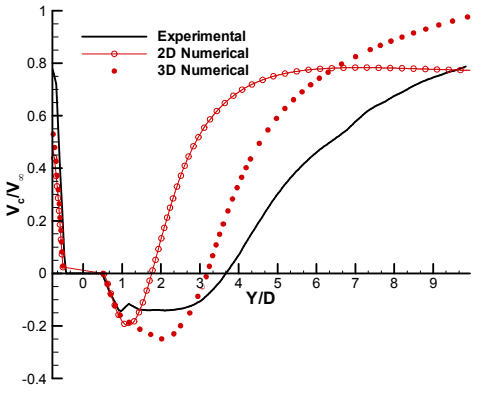

Figure 8. Variation of time-averaged wake centerline velocities with Ri

This is also clearly represented in Fig. 8, which shows the time-averaged wake centerline velocities for 2D numerical simulation comparing it to the experimental data and 3D numerical results. This indicates that the 2D simulation is unable to capture the flow phenomenon correctly. For the unheated cylinder case Ri=0.00, the velocity deficit is found to recover gradually with the increasing downstream distance around x/D>3 as expected Hu et al. [10]. With the increasing Richardson number, the stronger influence of buoyancy results in a stronger reversing flow near the trailing end of the cylinder. Consequently the strong recirculation zone is pushed further downstream and the recovery rate of the streamwise velocity deficit decreases (Hu et al. [10]). This can be explained more clearly by the time-averaged wake centerline velocities in Fig 9. The trend for the time-averaged centerline velocities from the present calculations gives a good agreement with the experimental observations Hu et al. [10]. According to the definition given by Hu et al. [10], wake closure length lc is the distance from the rear end of the heated cylinder to the point where the time-averaged mean velocity becomes zero and changes its sign. The wake closure length for unheated cylinder from the present result differs by almost 13% from the experimental result. Whereas for the heated cases of Ri=0.72 and Ri=1.05 it matches well within 10% with the experimental results.

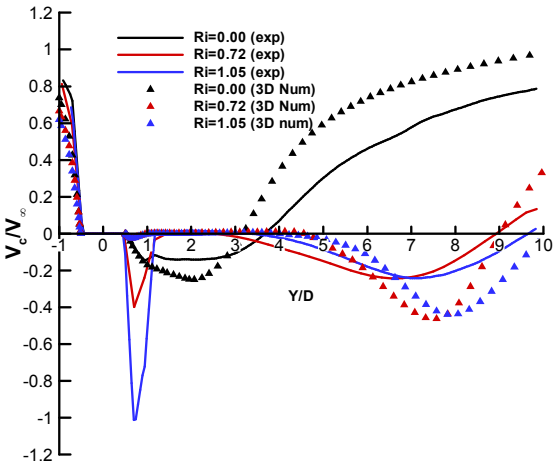

Figure 9. Variation of time-averaged wake centerline with Ri

C. Pressure Distribution and Time-averaged Drag Coefficient

The pressure distribution over the cylinder is shown in Fig. 11, for Ri=0.0, Ri=0.5 and Ri=1.05. It is known that the total drag comprises of drag due to the skin friction and pressure drop. As the temperature increases, the influence of buoyancy increases. Hence the drag due to the skin friction decreases marginally owing to the decreasing viscosity of the surrounding fluid while the drag due to the pressure drop increases substantially. Thus the drag due to skin friction can be neglected for higher Ri case[illegible] dominant in the total drag calculation. The mean pressure drag

$$\overline{D} \cong \int \overline{p} dA$$

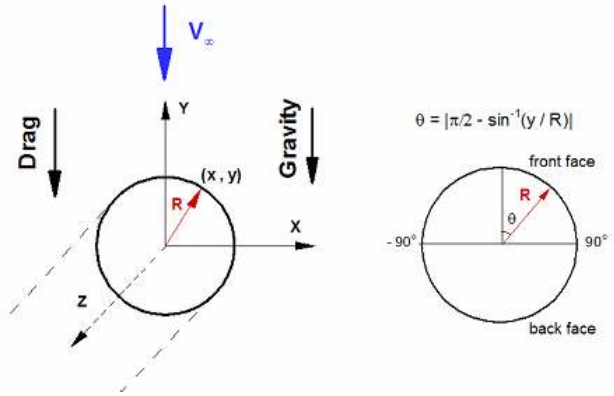

Figure 10. Schematic of pressure distribution over cylinder at symmetry plane.

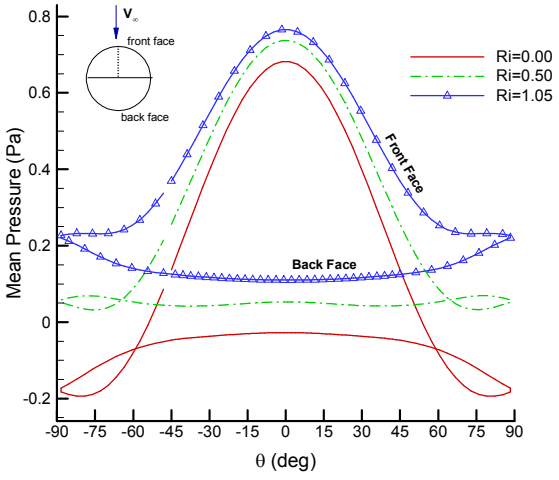

Figure 11. Mean Pressure distribution over the cylinder in contra flow

Fig. 11, clearly represents that the $\overline{D}$ increases as *Ri* increases. Due to the increasing effect of buoyancy with higher temperature of the cylinder the separation point moves towards the upstream of the heated cylinder for *Ri>0.3* which is indirectly depicted in Fig. 11. This flow separation results in a wider wake for the heated cylinder than the unheated cylinder. Consequently the drag is higher when the cylinder is heated than when it is unheated, due to higher contribution from the form drag. The drag coefficient C_d is averaged over a number of vortex shedding cycles to obtain $\overline{C_d}$ since $\overline{D}$ is also averaged.

$$\overline{C_d} = \frac{2\overline{D}}{\rho_\infty V_\infty{}^2 A} \qquad (9)$$

It is observed in Fig. 12 that the $\overline{C_d}$ for Ri=0.3 is much lower than *Ri=0.0*. This is explained by Hu et al. [10], and it is due the effect of buoyancy being still weak. But as discussed earlier, when the *Ri>0.3* the effect of buoyancy becomes considerable and that affects the drag coefficient. As seen in Fig. 12, the numerical calculation for *Ri=0.50* seems to over predict the $\overline{C_d}$ by almost 15%. This could mean that the critical *Ri* at which the buoyancy effects become significant would be between 0.3 and 0.5. For *Ri=0.72* and *Ri=1.05* it under predicts the C_d by 11.25% and 10% respectively.

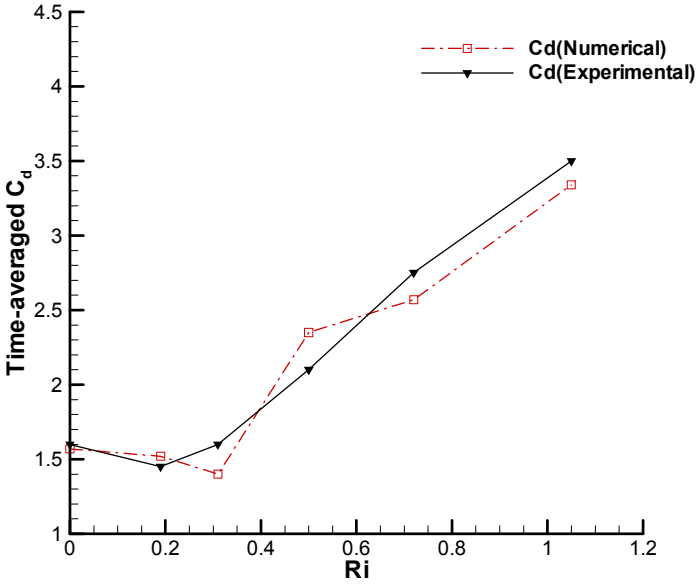

Figure 12. Time-averaged Drag Coefficient as function of Ri.

D. Vortex Shedding Frequency

The phenomenon of vortex shedding from the bluff bodies has been studied since the pioneering work of Von Karman and Strouhal. The Strouhal Number is the measure of the oscillating fluid flow phenomenon in the wake region, and defined using the flow parameters by the following relation:

$$St = \frac{f \times D}{V_\infty} \qquad (10)$$

where is f the vortex shedding frequency, D is the diameter of the cylinder and V_∞ is the free steam velocity. In the present study the Strouhal number for the six varied cases is deduced from the signal traces of the temporal lift force coefficient Strouhal Number and is compared with some of the existing experimental and numerical investigations for Re=100 and *Ri=0.0*. This can be seen in Table 6. A good agreement can be noticed with the studies listed in this table. Thus for the unheated cylinder case the 2D calculations produce a good accuracy in terms of vortex shedding frequency. However as we increase the temperature of the cylinder (*Ri>0.19*), we see variations in the results from the 2D and 3D calculations. This is represented in Table 7 and Fig. 15. The results obtained for the heated cylinder case where the *Ri>0.00*, are compared to the results from Hu et al. [10] and Chang and Sa [8]. In the discussion for the numerical methodology earlier, we have discussed that all the fluid properties like density, viscosity, thermal conductivity and thermal expansion coefficient varying as a function of the temperature.

Based on the same idea, Dumouchel et. al [11] and Wang et al. [12], introduced the concept of effect Reynolds number as a function effective temperature defined as $T_{eff} = T_\infty + 0.28\left(T_w - T_\infty\right)$ which can be used to predict the vortex shedding frequency. However it is already brought to our attention by Hu et al. [10] that this idea is inapplicable to our present study since Dumouchel et. al [11] and Wang et al. [12] have studied the effect of heating

only for very small temperature differences ie. *Ri<0.02*. For small temperature differences the buoyancy effects can be studied using a Boussinesq approximation in the governing equations. This approximation cannot be implemented for large temperature differences as is the case in the present study.

Table 6. Comparison of *St* at *Ri=0.0*

Re	*Researcher*	*Method*	*St*
130	Present Study	2D-Cal	0.171
		3D-Cal	0.173
	Hu (2004)	Exp	0.170
100	Noto and Fujimoto(2006)	2D-Cal	0.168
	Zhang(1995)	2D-Cal	0.173
	Persillon(2001)	3D-Cal	0.164
	Sa and Chang(1990)	2D-Cal	0.157
	Williamson (1996)	Exp	0.204

Table 7. Comparison of *St* for various *Ri*

Ri	*St (Exp)*	*St (2D Num)*	*St (3D Num)*
0.0	0.171	0.170	0.172
0.19	0.1661	0.162	0.163
0.3	0.152	0.160	0.150
0.5	0.119	0.152	0.127
0.72	0.105	0.142	0.109
1.05	0.1025	0.125	0.1045

The results shown in Table 7 and Fig. 13, reveal that the 2D simulation for the flow over heated cylinder does not produce accurate results for vortex shedding with *Ri>0.3* in comparison to the experimental data of Hu et al. [10]. Infact the 2D numerical calculations seem to over predict the vortex shedding frequency for *Ri>0.3*. Whereas the 3D numerical calculations match very close, almost within 2.0-10.0 % with the experimental results with the increasing *Ri*. This forms the first step to understanding the possibility of 3D transition being extended for the Re=130 and *Ri>0.02* and we could conclude that 2D numerical simulations are certainly incapable of capturing the flow physics due to the buoyancy effects. For the same reason all the results have been explained only for 3D numerical simulations and not 2D numerical simulations.

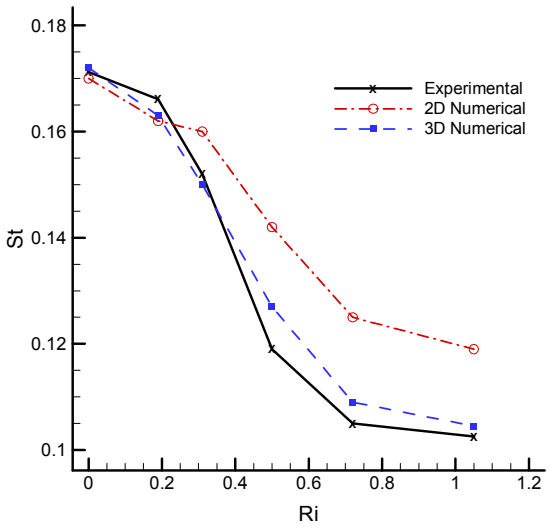

Figure 13. Strouhal number for various Ri

The 3D transition and its relation to the vortex shedding for higher Ri will be more clear from the explanation in the following results. The difference in the decreasing trend between the experimental data and the numerical results of Chang and Sa [8] has been explained in detail by Hu et al. [10] For lower Richardson number, *Ri=0.31*, the vortex shedding pattern in the wake of the heated cylinder is similar to the pattern for the unheated cylinder. However the vortex shedding was found to be delayed and occurs further downstream with the increasing *Ri=0.5*. Although the numerical simulation by Chang and Sa [8] involved a 2D calculation, it seems to give better agreement with the experimental results than the 2D calculation for the present numerical study. Chang and Sa [8] have used a Boussinesq approximation, although the temperature differences are high, while solving the governing equations. This assumption is not feasible here as explained earlier and is evident in the other results by Chang and Sa [8] which cannot predict the buoyancy effect clearly.

E. Averaged Nusselt Number

The knowledge of the heat transfer coefficients at low Re is invaluable to designers and engineers. Here the averaged Nusselt number is the parameter of interest.

$$\overline{Nu} = \frac{hD}{k} = \frac{\overline{Q}D}{A^2 k(T_w - T_\infty)} \tag{11}$$

Here $\overline{Nu}$ is the averaged Nusselt number and $\overline{Q}$ is the averaged heat transfer rate. In this case we have a mixed convection resulting from the heat transfer by forced and free convection. The experimental data by Hu et al. [10] suggests that with the increasing Ri, $\overline{Nu}$ decreases. Fig. 14, shows the comparison of the results obtained from the present numerical study with the experimental results of Hu et al. [10]. The numerical results indicate the same trend as the experimental results. However it seems to over predict the $\overline{Nu}$ by around 10%. But the results clearly indicate that with the increasing Ri the effect of buoyancy increases. The forced convection and free convection are in opposite direction which results in the decreasing trend.

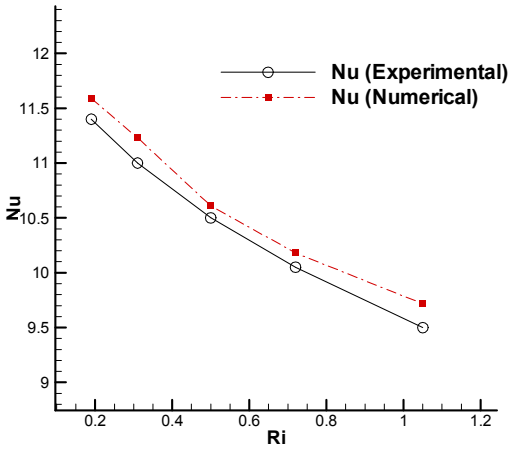

Figure 14. Variation of averaged Nusselt for various Ri.

F. Thermal effect of buoyancy on 3D wake flow

For flows with small AR (less than 28) or finite length of cylinders, we would see a 3D transition of wake behavior different from that for the cylinders with infinite length or large AR. From the studies by Williamson [1], for the unheated cylinders with large AR the transition regime would be between 190-250. However this transition regime is extended and/or delayed for a cylinder with small AR with "no-slip" walls Mittal [2]. This suggests that besides Reynolds number, the end-effects and aspect-ratio (AR) plays a major role in the nature of the flow behind a cylinder. In the present study, the cylinder with a small AR = 7 has been considered. In addition to this, a no-slip boundary condition has been implemented for the walls. These factors significantly affect the wake behavior of the flow although the Re=130 does not lie in the usual transition regime of 190-250. Instead we see a 3D wake behavior for flow at this Re which is also depicted in various results compared above. We have already discussed the influence of heat input and buoyancy on the wake behavior in terms of the vortex shedding frequency, time-averaged centerline velocities, time-averaged drag coefficient and Nusselt number. We have also mentioned that all these results are also influenced significantly by the end conditions which lead to 3D wake behavior.

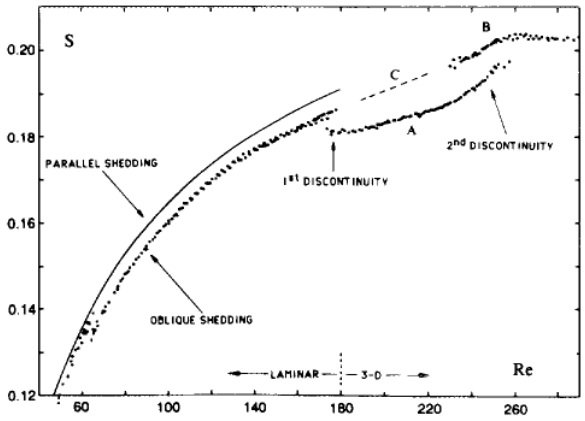

Figure 15. Strouhal-Reynolds number relationship over laminar and three-dimensional transition regimes Williamson [1]

Fig. 16-22, show the instantaneous pressure, velocity components and vorticity components for the temporally periodic flow for *Ri=0.0* when the cylinder is not heated. We are looking at the yz section passing through the axis of the cylinder. We can observe the spatial development of the boundary layer at the wall due to the no-slip boundary condition and we do not observe vortex shedding here due to the presence of the boundary layer. It is clear that the wake becomes very unstable because of the heating. This would suggest that heating and small aspect ratio would prolong or delay onset of transition regime.

The transition to the three-dimensionality in the wake can be conveniently illustrated using the relationship between the Strouhal and Reynolds numbers. In the Fig. 15, Williamson [1] shows that the first discontinuity of the Strouhal frequency occurs at Re at 180-190(mode A). The wake in this mode is associated with vortex loops and formation of streamwise vortex pairs due to the formation of primary vortices. The wavelength of the vortex deformations is 3-4 cylinder diameters. With the increasing Re from 230-260, we see another discontinuity (mode B) with the wavelength of streamwise vortex structures as one cylinder diameter approximately.

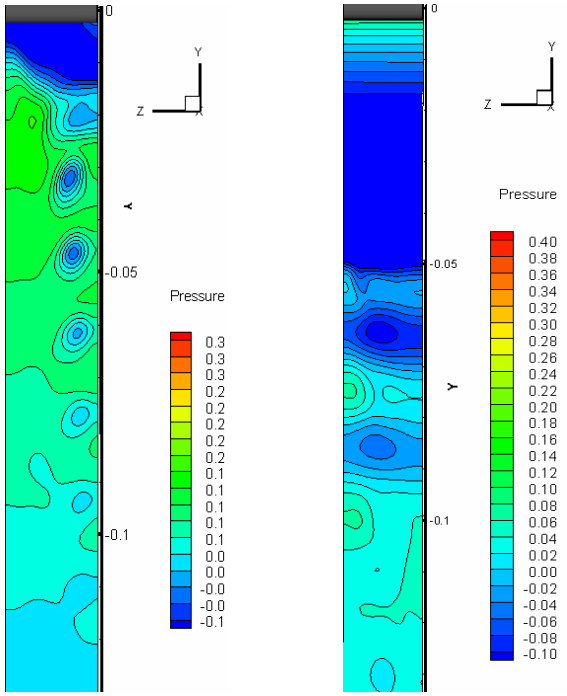

(a) Ri=0.00 **(b) Ri=1.05**

Figure 16. Instantaneous pressure contours on yz plane

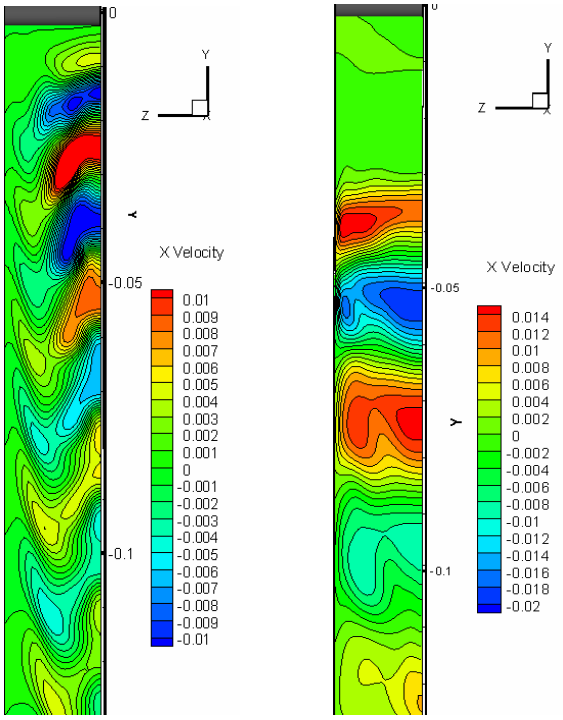

(a) Ri=0.0 **(b) Ri=1.05**

Figure 17. Instantaneous x-velocity component at yz plane

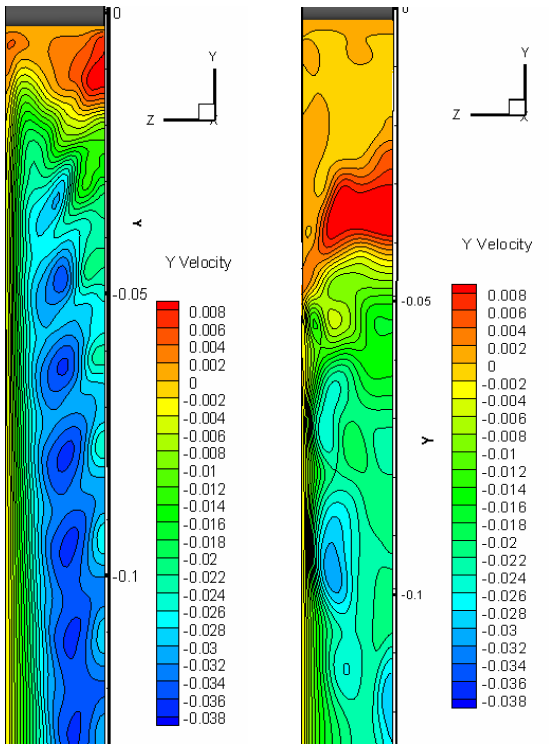

(a) Ri =0.0 **(b) Ri =1.05**

Figure 18. Instantaneous y-velocity component at yz plane

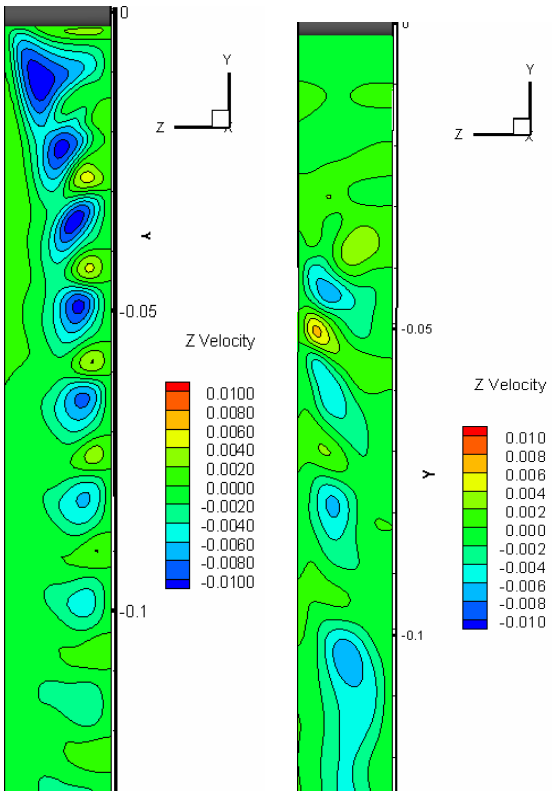

(a) Ri =0.0 **(b) Ri =1.05**

Figure 19. Instantaneous z-velocity component at yz plane

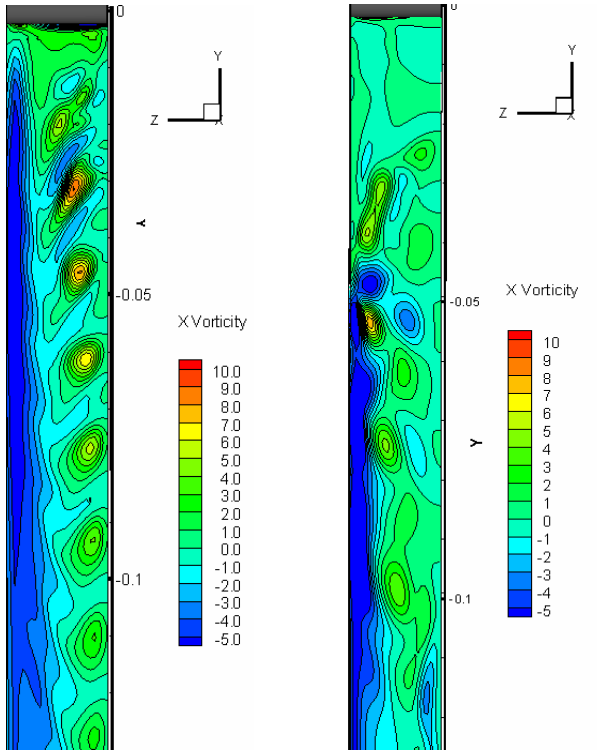

(a) Ri =0.0 **(b) Ri =1.05**

Figure 20. Instantaneous x-vorticity component at yz plane

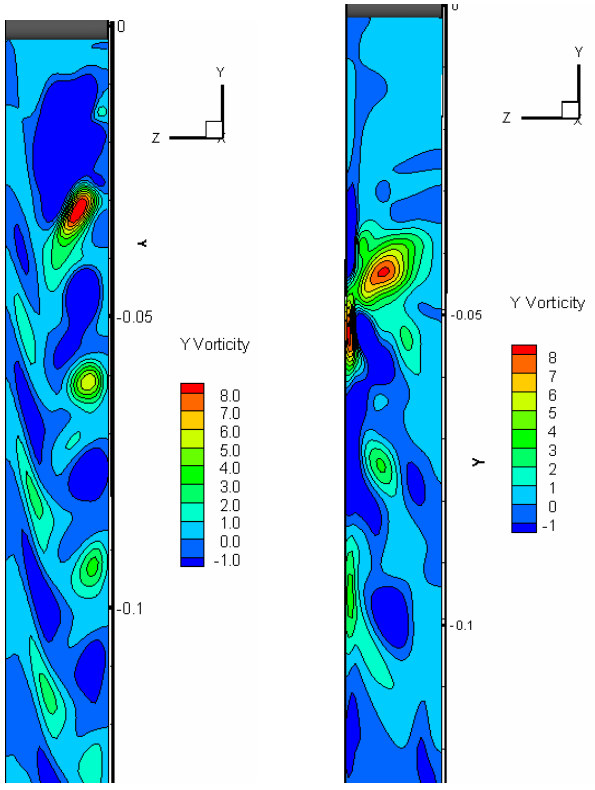

(a) Ri =0.0 **(b) Ri =1.05**

Figure 21. Instantaneous y-vorticity component at yz plane

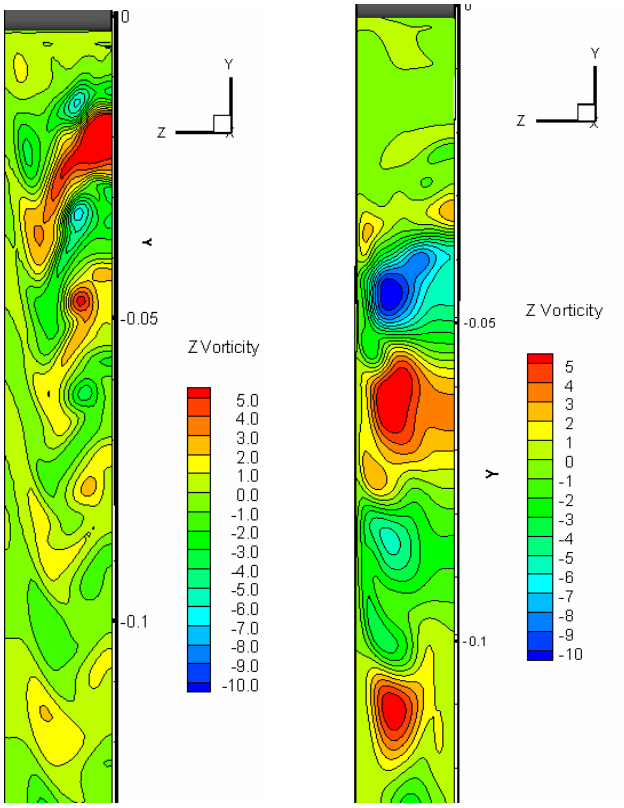

(a) Ri=0.0 **(b) Ri=1.05**

Figure 22. Instantaneous z-vorticity component at yz plane

During the transition, the time histories of the lift forces are associated with two peaks: a peak at lower frequency that corresponds to mode A that gradually diminishes and a peak at higher frequency that takes over as the Re increases. Williamson [1] attributes this to the intermittent swapping between the two modes. A similar trend is observed for *Ri=1.05* shown in Fig. 23 and Fig. 24. The temporal history of lift force shows two different modes. One of the modes diminishes with time and the other one becomes dominant. In this case, the transition that would start in Re range 190-250 seems to be extended because of heating. However more work is needed to understand the effect of heating and small aspect ratios on transition.

The detailed study of the vortex patterns and wake instability would aid in the understanding of the same. In addition to this, a large number of *Ri* would give more insight into this phenomenon.

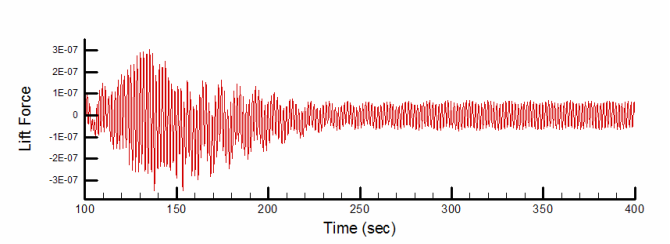

Figure 23. Temporal history of lift force for Ri=1.05

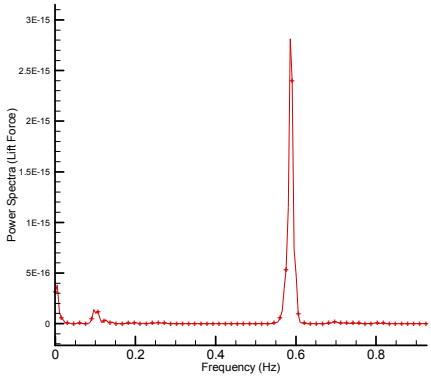

Figure 24. Power spectra of lift force time history for Ri=1.05

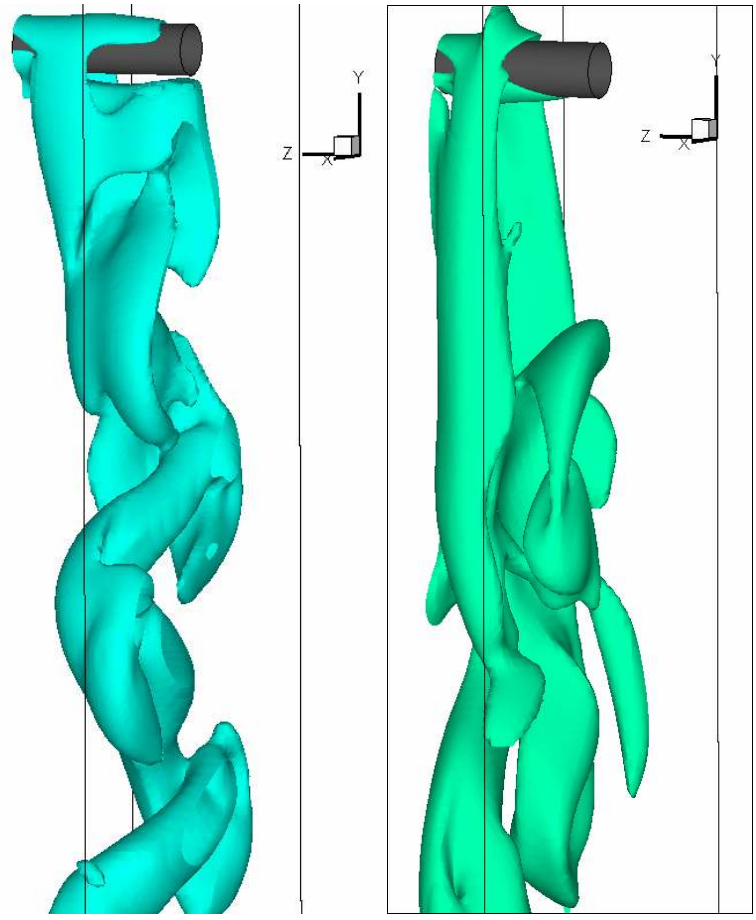

(a) Ri = 0.0 **(b) Ri = 1.05**

Figure 25. Iso-surface for x-vorticity component (=0.5) for the unsteady solution

IV. CONCLUDING REMARKS

The influence of buoyancy opposing the flow direction due to mixed convection is numerically simulated for flow past a circular cylinder with small aspect ratio (AR=7) at Re=130. The Richardson number based on the temperature of the cylinder varies between *Ri=0.0 to 1.05*. Numerical results are generated by solving time-accurate finite volume method based unsteady compressible Navier-Stokes equations. Most of the previous studies have been conducted with the slip boundary conditions. In the present study the influence of heating in addition to small aspect ratio of the cylinder and no-slip wall boundary conditions on the pressure distribution, time-averaged drag co-efficient, time-averaged centerline velocities, Strouhal number, averaged Nusselt number and transition mechanism has been numerically investigated and validated with the available experimental results. Some of the broad conclusions can be outlined as follows:

- Due to the small aspect ratio with no-slip walls, we see a 3D wake for Re=130 unlike the large aspect ratio.
- Under the influence of buoyancy the flow separation occurs earlier than when the cylinder is not heated. This results in a wider and longer wake for the heated cylinder and a narrower wake for the unheated cylinder.
- The wake closure length increases with the Richardson number and consequently the averaged drag coefficient is higher for the heated cylinder. The drag has a significant contribution from the pressure drop whereas the drag due to skin friction is negligible.
- The vortex shedding frequency in terms of Strouhal number almost decreases with the increasing Richardson.
- Averaged Nusselt number follows the same decreasing trend as the experimental results with the increasing Richardson number.
- Preliminary analysis for influence of buoyancy on the wake behavior at Re=130 for cylinder in contra flow suggests that heating instigates an early transition. It is interesting to observe the significance of small aspect ratio

and end effects in addition to the heating, on the transition mechanism. However much more work needs to be done over a larger range of temperature and Reynolds number to determine the onset of transition before any certain conclusions can be drawn. Detailed analysis of the vortex shedding patterns and vortex dislocations can aid to the understanding of various modes in transition regime for a heated cylinder.

References

[1] Williamson, C. H. K., "Vortex Dynamics in the Cylinder Wake", *Annual Review of Fluid Mechanics*, Vol. 28, pp477-526, (1996).

[2] Mittal, S., "Computation of three-dimensional flows past circular cylinder of low aspect ratio", *Physics of Fluids*, Vol. 13, No. 1, pp177-191, (2001).

[3] Hatton , A. P., James, D. D., Swire, H. W. , "Combined Forced and Nature Convection with Low Speed Air Flow over Horizontal Cylinders", *Journal of Fluid Mechanics*, Vol. 42, pp17-30, (1970).

[4] Ooesthuizen, P. H., and Madan, S., "Combined convective heat transfer from horizontal circular cylinders in air", *Transactions of ASME Journal of Heat Transfer,* Vol. 92, pp194-196, ASME (1970).

[5] Jain, P.C., and Lohar, B. L., "Unsteady mixed convection heat transfer from a horizontal circular cylinder," *Transactions of ASME Journal of Heat Transfer*, Vol 101, pp126-131, ASME (1979).

[6] Noto, K., and Matsumoto, M., "Generation and suppression of the Karman vortex street upon controlling surface temperature of a cylinder," *Proceedings of Numerical Methods Laminar and Turbulent Flows*, Vol. 7, pp671-678, (1991).

[7] Badr, H. M., "Laminar combined convection from a horizontal cylinder in parallel and contra flow regimes," *International Journal of Heat and Mass Transfer*, Vol 27, No. 1, pp15-27, (1984).

[8] Chang, K. S., and Sa, J. Y., "The effect of buoyancy on vortex shedding in the near wake of a circular cylinder," *Journal of Fluid Mechanics*, Vol. 220, pp253-260, (1990).

[9] Kieft, R. N., Rindt C. C. M. and Steenhoven A. A. Van., "The Wake Behavior Behind a Heated Horizontal Cylinder," *Experiments in Thermal and Fluid Science*, Vol. 19, pp193-193, (1999).

[10] Hu, H., and Kochesfahani M., "The Wake Behavior behind a Heated Cylinder in Forced and Mixed Convection Regimes," *ASME Summer Heat Transfer Conference,* ASME, San Francisco, CA, (2005).

[11] Dumouchel F., J. C. Lecordier and P. Paranthon P., "The Effective Reynolds Number of a Heated Cylinder", *International Journal of Heat and Mass Transfer*, Vol. 40, N0. 12, pp1787-1794, (1998)

[12] Wang, A., Travnick Z. and Chia K., "On the Relationship of Effective Reynolds Number and Strouhal Number for the Laminar Vortex Shedding of a Heated Circular Cylinder", *Physics of Fluids*, Vo. 12, No. 6, pp1401-1410,(2000)

[13] Incropera, F.P., and DeWitt, D. P., *Fundamentals of Heat and Mass Transfer, 5th Edition*,(2002)

[14] Joshi, N. D., and Sukhatme, S. P., "An analysis of combined free and forced convection heat transfer from a horizontal circular cylinder to a transverse flow", *Transactions of ASME Journal of Heat Transfer*, Vol. 92, pp194-196, (1970).

[15] Sparrow, E. M., and Lee, L., "Analysis of a mixed convection about a horizontal cylinder*," International Journal of Heat and Mass Transfer*, Vol. 19, pp229-231, (1976).

[16] Patnaik, B. S. V. P., Seetharamu, K. N., and Aswatha Narayana, P. A., "Simulation of laminar confined flow past a circular cylinder with integral wake splitters involving heat transfer," *International Journal of Numerical Methods for Heat and Fluid Flow*, Vol 6, No 4, pp65-81, (1996).

[17] Williamson, C. H. K., "Defining a universal and continuous Strouhal relationship for the laminar vortex shedding of a circular cylinder," *Physics of Fluids*, Vol. 31, No. 10, pp2742-2744, (1988).

[18] Fluent Notes and User Manual (2003)

[19] Hatanaka, K., and Kawahara, M., "Numerical study of vortex shedding around a heated/cooled circular cylinder by the three step Taylor-Galerkin method," *International Journal for Numerical Methods in Fluid,* Vol. 17, pp349-364, (1993).